Biallelic CHP1 mutation causes human autosomal recessive ataxia by impairing NHE1 function

OPEN

Natalia Mendoza-Ferreira, MSc
Marie Coutelier, MD, PhD
Eva Janzen, MSc
Seyyedmohsen Hosseinibarkooie, PhD
Heiko Löhr, PhD
Svenja Schneider, MSc
Janine Milbradt, MSc
Mert Karakaya, MD
Markus Riessland, PhD
Christian Pichlo, MSc
Laura Torres-Benito, PhD
Andrew Singleton, PhD
Stephan Zuchner, MD
Alexis Brice, MD
Alexandra Durr, MD, PhD
Matthias Hammerschmidt, PhD
Giovanni Stevanin, PhD
Brunhilde Wirth, PhD

Correspondence to Prof. Dr. Wirth: brunhilde.wirth@uk-koeln.de

ABSTRACT

Objective: To ascertain the genetic and functional basis of complex autosomal recessive cerebellar ataxia (ARCA) presented by 2 siblings of a consanguineous family characterized by motor neuropathy, cerebellar atrophy, spastic paraparesis, intellectual disability, and slow ocular saccades.

Methods: Combined whole-genome linkage analysis, whole-exome sequencing, and focused screening for identification of potential causative genes were performed. Assessment of the functional consequences of the mutation on protein function via subcellular fractionation, size-exclusion chromatography, and fluorescence microscopy were done. A zebrafish model, using Morpholinos, was generated to study the pathogenic effect of the mutation in vivo.

Results: We identified a biallelic 3-bp deletion (p.K19del) in *CHP1* that cosegregates with the disease. Neither focused screening for *CHP1* variants in 2 cohorts (ARCA: N = 319 and NeurOmics: N = 657) nor interrogating GeneMatcher yielded additional variants, thus revealing the scarcity of *CHP1* mutations. We show that mutant CHP1 fails to integrate into functional protein complexes and is prone to aggregation, thereby leading to diminished levels of soluble CHP1 and reduced membrane targeting of NHE1, a major Na^+/H^+ exchanger implicated in syndromic ataxia-deafness. Chp1 deficiency in zebrafish, resembling the affected individuals, led to movement defects, cerebellar hypoplasia, and motor axon abnormalities, which were ameliorated by coinjection with wild-type, but not mutant, human *CHP1* messenger RNA.

Conclusions: Collectively, our results identified *CHP1* as a novel ataxia-causative gene in humans, further expanding the spectrum of ARCA-associated loci, and corroborated the crucial role of NHE1 within the pathogenesis of these disorders. ***Neurol Genet*** **2018;4:e209; doi: 10.1212/NXG.0000000000000209**

GLOSSARY

ARCA = autosomal recessive cerebellar ataxia; **CaP-MN** = caudal primary motor neuron; **cDNA** = complementary DNA; **EGFR** = epidermal growth factor receptor; **GFP** = green fluorescent protein; **HMW** = high molecular weight; **HPRT** = hypoxanthine-guanine phosphoribosyltransferase; **HSP90** = heat shock protein 90; **KO** = knockout; **LKS** = Lichtenstein-Knorr syndrome; **LOD** = Logarithm of the odds; **mRNA** = messenger RNA; **MO** = Morpholino; **OE** = overexpression; **RT-PCR** = reverse transcription PCR; **SEC** = size-exclusion chromatography; **WB** = Western blot; **WES** = whole-exome sequencing; **WT** = wild type.

Autosomal recessive cerebellar ataxias (ARCAs) comprise a heterogeneous group of neurodegenerative disorders associating cerebellar degeneration to a variable combination of central or peripheral neurologic or nonneurologic signs.[1] Collectively, ARCAs have an estimated frequency of 1:20,000 and often show overlapping features with spastic paraplegias and peripheral neuropathies.[2–4] Approximately 40% of individuals with suspected ARCA remain genetically

From Institute of Human Genetics (N.M.-F., E.J., S.H., S.S., J.M., M.K., M.R., L.T.-B., B.W.), Center for Molecular Medicine Cologne, Institute for Genetics and Center for Rare Diseases Cologne, University of Cologne, Cologne, Germany; Institute for Zoology, Developmental Biology (H. L., M.H.), Institute of Biochemistry (C.P.), University of Cologne, Germany; Institut du Cerveau et de la Moelle épinière (M.C., A.B., A.D., G.S.), INSERM U 1127, CNRS UMR 7225, Sorbonne Universités, UPMC Univ Paris 06 UMRS 1127, France; Ecole Pratique des Hautes Etudes (M. C., G.S.), PSL Research University, Paris, France; Laboratory of Molecular and Cellular Neuroscience (M.R.), The Rockefeller University, New York, NY; Laboratory of Neurogenetics (A.S.), National Institute on Aging, National Institutes of Health, Bethesda, MD; John P. Hussman Institute for Human Genomics (S.Z.), University of Miami, Miller School of Medicine, FL; and APHP (A.B., A.D., G.S.), Hôpital de la Pitié-Salpêtrière, Centre de réference de neurogénétique, Paris, France.

Funding information and disclosures are provided at the end of the article. Go to Neurology.org/ng for full disclosure forms. The Article Processing Charge was funded by the authors.

undiagnosed,[2,3,5] implying that a large number of causative genes—usually the most rare and challenging to identify—still need to be uncovered.

Here, we report the identification and characterization of a novel ARCA causative mutation in *CHP1* (calcineurin homologous protein-1, NM_007236.4:c.52_54del: p.Lys19del). CHP1 serves as an essential cofactor of NHE1 (sodium/hydrogen exchanger 1),[6,7] a major regulator of intracellular ions and pH homeostasis.[8] Biallelic splice mutation of mouse *Chp1* leads to reduced NHE1 membrane targeting and degeneration of Purkinje cells, ultimately causing ataxia.[6] Similarly, mouse *Nhe1* (encoded by *Slc9a1*) knockout (KO) causes Purkinje cell loss, severe locomotor ataxia, and epilepsy,[9,10] while homozygous loss-of-function *SLC9A1* mutations in humans cause cerebellar ataxia and sensorineural hearing loss.[11] Therefore, we hypothesized that a mutation in CHP1, as a crucial regulator of NHE1,[6,7] could impair expression and targeting of the exchanger, resembling the pathogenesis in mice and humans. Taking advantage of the zebrafish model system for modeling ARCAs,[12–14] we generated a *chp1*-deficient zebrafish, which not only resembled the clinical features of the affected siblings but also corroborates the pathogenicity of the CHP1 hypomorphic Lys19del mutation in vitro and in vivo.

METHODS

Patient consents and standard protocol approvals. Informed consent was obtained from participants in accordance with French ethics regulations (Paris Necker ethics committee approval [RBM 01-29 and RBM 03-48] to A.B. and A.D.). Zebrafish procedures were approved by the local animal protection committee LANUV NRW; reference 84-02.04.2012.A251.

Whole-exome sequencing and whole-genome linkage analysis. Whole-exome sequencing (WES) of individuals 1, 2, 6, and 8 of family AAR-087 was performed on the Illumina HiSeq 2000 as paired-end 100bp reads after library preparation with the SureSelect Human All Exon 50 Mb V4 kit (Agilent Technologies. Santa Clara, California). ARCA and NeurOmics cohort WES and bioinformatic processing details are given in supplemental data. Whole-genome linkage analysis was performed using Illumina LINKAGE_12 microarrays (6090 single nucleotide polymorphism markers). Genotypes were determined by BeadStudio (Illumina, San Diego, CA) and analyzed with MERLIN 1.0.[15]

Expression vector generation and site-directed mutagenesis. Full-length human *CHP1* complementary DNA (cDNA) (NCBI: 11261) was cloned into 2 expression vectors: pcDNA3.1/CT-V5His-TOPO and pcDNA3.1/CT-green fluorescent protein (GFP)-TOPO following the manufacturer's instructions (Life Technologies, Darmstadt, Germany). K19del mutation was introduced by site-directed mutagenesis (see primers, table e-1 at links.lww.com/NXG/A29), following QuikChange kit instructions (Agilent Technologies, Santa Clara, CA). Clones were verified by Sanger sequencing.

Cell culture and transfection. HEK293T (human embryonic kidney), HeLa (human cervical carcinoma), PC12 (murine pheochromocytoma), and N2A (murine neuroblastoma) cells were grown, maintained, and differentiated following standard protocols. Cells were transfected with plasmid DNAs, including control empty vectors, using Lipofectamine2000 (Life Technologies) and harvested after 24, 48, or 72 hours for RNA and protein isolation.

Semiquantitative reverse transcription PCR. RNA was extracted using the RNeasy kit (Qiagen, Hilden, Germany), and concentrations were determined using the RiboGreen method (Life Technologies). Three hundred nanograms of RNA were reverse transcribed to cDNA with the Quantitect Reverse Transcription Kit (Qiagen). PCR was performed with low cycle number (N = 24) and as multiplex with the housekeeping gene hypoxanthine-guanine phosphoribosyltransferase (*HPRT*) (see primers, table e-1, links.lww.com/NXG/A29). Densitometric analysis was performed with ImageLab 5.2.1 (Bio-RAD).

Cellular fractionation, size-exclusion chromatography, and Western blot. After 48 hours of transfection, HEK293T cells were processed with the Subcellular Protein Fractionation Kit for cultured cells (Thermo Scientific, Schwerte, Germany) following the manufacturer's instructions. Size-exclusion chromatography (SEC) was performed with a Superose, 10/300-GL column connected to the ÄKTA-pure FPLC system (GE Healthcare, Freiburg, Germany). Sample preparation and column calibration details are given in supplemental data. Protein lysate preparation for Western blot (WB), sodium dodecyl sulfate-polyacrylamide gel electrophoresis, and transfer were performed according to the standard protocols. Antibodies used for immunologic protein detection are listed in table e-2, links.lww.com/NXG/A29. Densitometric analysis was performed with ImageLab 5.2.1 (Bio-RAD).

Fluorescence immunostaining. N2A, PC12, and HeLa cells transiently expressing pcDNA3.1-CHP1-GFP vectors were seeded in laminin-coated coverslips (Thermo Scientific, Schwerte, Germany) to preserve neurite-like structures, if necessary. After 24 hours of transfection and 4–5 days of differentiation, cells were immunostained as described in reference 16. Antibodies used are listed in table e-2, links.lww.com/NXG/A29.

Zebrafish experiments. Experiments for caudal primary motor neuron (CaP-MN) analysis were performed with the transgenic line *tg(mnx1-GFP)ml2TG* (synonym TL/EK-*hb9-GFP*[17]). Cerebellar analyses were performed in the wild-type (WT) TL/EK line. Control and *chp1* Morpholinos (MO) (against translational start codon, table e-1, links.lww.com/NXG/A29) were designed and purchased from GeneTools, LLC (Philomath, OR). WT and mutant human *CHP1* cDNAs were introduced into a pCS2+ vector for in vitro transcription of capped messenger RNAs (mRNAs), performed as previously described.[16] Zebrafish protein lysates for WB were prepared following the protocol described in reference 18 with modifications, explained in e-Methods. Embryo injections and CaP-MN immunostaining were performed as previously described.[16] For cerebellar immunostainings, ~72-hpf zebrafish larvae were fixed overnight in Dent solution and processed as described in reference 12. Antibodies

used are listed in table e-2, links.lww.com/NXG/A29. Neurologic readouts quantification, movement analysis, and imaging procedures are given in supplemental data.

Microscopy. Images were acquired using a Zeiss AxioImager M2 microscope equipped with ApoTome2 system to mimic confocality (Zeiss, Jena, Germany). Zebrafish CaP-MN and cerebellum images were acquired as Z-stacks and processed using ZEN software. Colocalization analyses were performed with ZEN. Representative images were processed using ImageJ. All experiments were blinded.

Protein modeling. Protein structures of free CHP1 (2CT9) and NHE1-bound CHP1 (2E30) were acquired from RCSB Protein Data Bank (http://www.rcsb.org/pdb/home/home.do). Cartoon representations were generated using PyMOL 1.5.0.4.

Statistics. Statistical analyses were performed using GraphPad Prism 6. Two-tailed Student t tests, χ^2, and Fisher exact statistics tests were performed. Levels of statistical significance are given in GraphPad format ($*p \leq 0.05$, $**p \leq 0.01$, $***p \leq 0.001$, and $****p \leq 0.0001$). Specific tests, sample size, data representation, and p values are indicated in figure legends.

RESULTS Identification of a 3-bp deletion in *CHP1* causes autosomal recessive spastic ataxia. Two of 6 siblings of a consanguineous Moroccan family (figure 1A) developed autosomal recessive spastic ataxia with onset during the first decade of life. They show gait instability with moderate cerebellar atrophy (figure 1B) and upper and lower motor neuron involvement, intellectual disability, growth retardation, slow ocular saccades, and ovarian failure in the female proband. Positive pyramidal and cerebellar signs along with additional clinical features are summarized in table e-3, links.lww.com/NXG/A29 and extendedly described in supplemental data.

WES of individuals 1, 2, 6, and 8 yielded an average of 84,556,652 sequence reads per sample, of which >98.5% could be aligned to the reference sequence. Mean coverage was 77-fold, with 78.9% of the targeted sequence covering more than 20×. Twelve variants, all located within the linked regions (multipoint logarithm of the odds [LOD] score >−2), segregated recessively

Figure 1 Phenotype and genotype of an undiagnosed family with autosomal recessive spastic ataxia

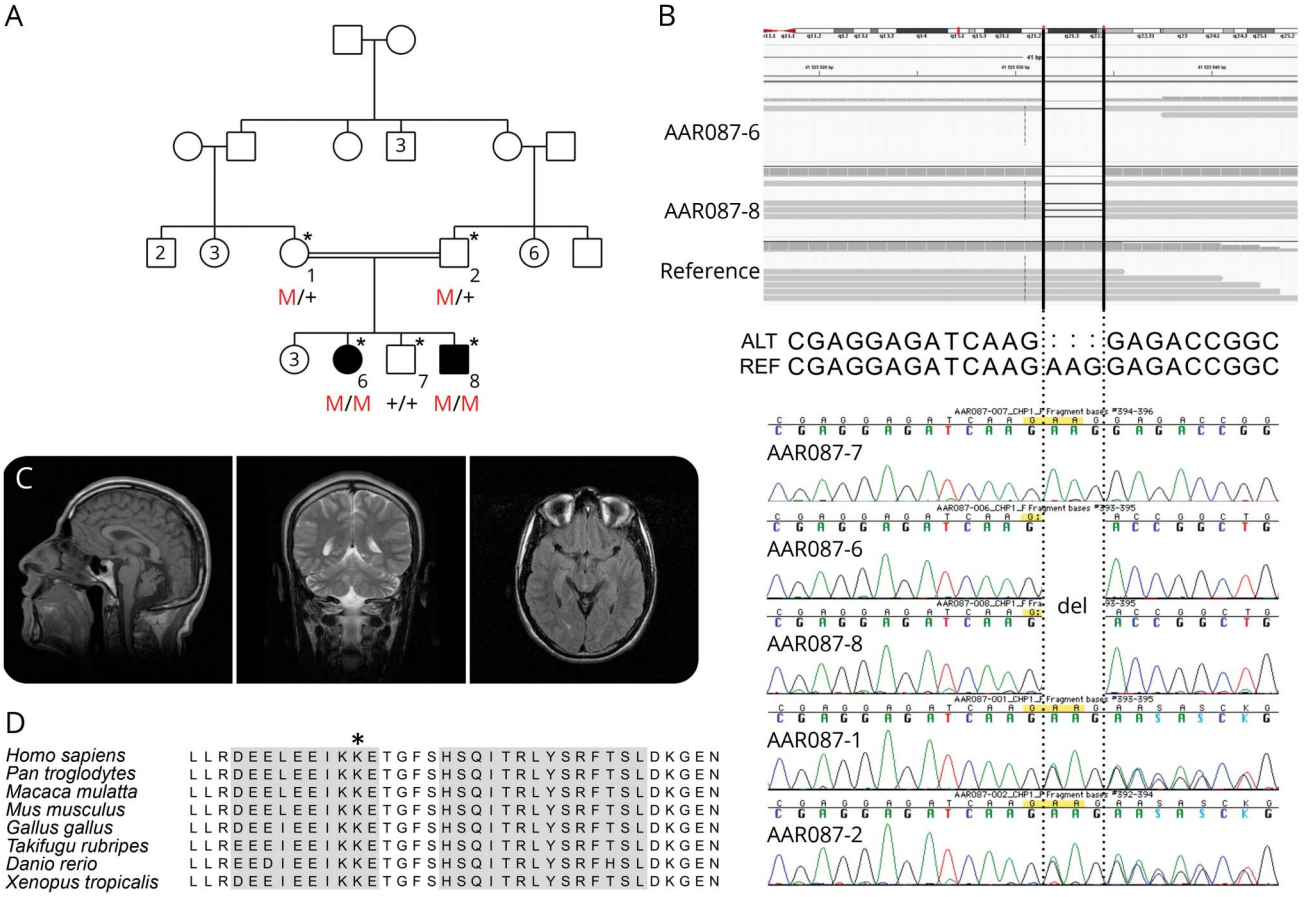

(A) Pedigree of the family showing the segregation of the CHP1 p.K19del mutation (red M; "+" denotes the reference allele). (B) *CHP1* next-generation sequencing reads show the homozygous NM_007236:c.52_54del: p.K19del variant for individuals IV-6 and IV-8. Sanger sequencing pherograms show homozygosity for the 3-bp deletion in both patients and heterozygosity in both parents; the unaffected sibling IV-7 shows the homozygous reference sequence. (C) Brain MRI of proband of individual IV-8 at 22 years of age. Sagittal (left panel) and coronal (middle panel) sections of T1-weighted images are shown. Hypoplasia of the posterior and nodular regions of the cerebellar vermis, but not of the hemispheres, is observed. An axial fluid-attenuated inversion recovery section (right panel) shows no evident white matter abnormalities. (D) Protein sequence alignment of CHP1 orthologs shows high conservation in the region including the K19del mutation (marked with asterisk). Gray indicates α-helical protein structure.

in the family (table e-4, links.lww.com/NXG/A29, and figure e-1, A and B, links.lww.com/NXG/A30). Further filtering based on alternate allele homozygosity and weak mutation effect prediction excluded 5 variants (table e-4, links.lww.com/NXG/A29). Of these, a biallelic 3-bp deletion in *CHP1* (NM_007236.4:c.52_54del:p.Lys19del), hereafter defined as K19del, was validated by Sanger sequencing (figure 1C) and further selected as a top disease candidate since (1) it is located in the largest nonexcluded region on chromosome 15, where the maximum LOD score is reached, (2) it is absent from all public databases, (3) the mutation affects an amino acid highly conserved across species (figure 1D), (4) a point mutation reported in mouse *Chp1*, causing aberrant splicing and reduced full-length transcripts, leads to degeneration of Purkinje cells and ataxia,[6] (5) CHP1 assists posttranscriptional glycosylation and membrane localization of NHE1; a major Na^+/H^+ exchanger listed in the ataxia-ome,[19] (6) KO of mouse *Nhe1* also cause ataxia,[10] and (7) mutations in *NHE1* cause ataxia-deafness Lichtenstein-Knorr syndrome (LKS).[11] Neither focused screening for CHP1 variants in 2 large cohorts, namely ARCA (N = 319) and NeurOmics (individuals with various neuromuscular diseases N = 657) nor GeneMatcher[20] interrogation revealed any additional variant in CHP1, fulfilling our pathogenic selection criteria (table e-5, links.lww.com/NXG/A29).

Endocrine dysfunction is CHP1 independent. The syndromic presentation of ataxia with hypergonadotropic hypogonadism was first described in 1908[21,22]; nonetheless, the genetic basis of this combination, except for few successful studies,[12,23] remains elusive. The female proband of this study presented with ovarian failure; however, neither *Chp1 vacillator* nor *Nhe1*-depleted female mice were reported as infertile. Our analysis of uteri from *vacillator* mice showed neither uterus nor ovarian impairments (data not shown). We speculated that a *CHP1*-independent mutation might account for this defect, further clarifying the *CHP1* family pathogenic landscape. WES revealed a homozygous variant (c.859C>T, p.G258E) in Basonuclin-1 (*BNC1*), which encodes a protein expressed only in reproductive germ cells with an essential function in oogenesis and spermatogenesis[24,25] (table e-4, links.lww.com/NXG/A29). *Bnc-1* null mice are sex-differentially affected, with females presenting complete infertility and subfertile males exhibiting smaller testes and reduced sperm motility.[24,25] Furthermore, a pathogenic copy number variant including the *BNC1* gene was recently detected in a retrospective study of spontaneous premature ovarian failure susceptibility.[26]

CHP1-K19del mutation alters protein solubility. To investigate the effect of CHP1-K19del, we examined the expression of CHP1-WT and CHP1-K19del-V5-tagged proteins in transiently transfected HEK293T cells by WB. Time-course analysis revealed reduced CHP1-K19del-V5 expression, whereas CHP1-WT-V5 exhibited higher levels over 72 hours of overexpression (OE) (figure 2A and figure e-2A). Semiquantitative reverse transcription PCR (RT-PCR) showed no differences between WT and mutant *CHP1* transcripts (figure 2B and figure e-2B, links.lww.com/NXG/A30), thus excluding a transcriptional impairment.

Next, we assessed the distribution of CHP1-WT and mutant in soluble and insoluble fractions. Compared with CHP1-WT-V5 levels, CHP1-K19del-V5 was ~62% reduced in the soluble fraction and increased by ~68% in the insoluble fraction, respectively (figure 2C). Similar results were seen in N2A cells (figure e-2C, links.lww.com/NXG/A30). Together, these observations hint toward defects in protein localization, solubility, or stability of the CHP1 mutant form which, alone or in combination, might explain the reduced levels of soluble protein.

Mutant CHP1 is prone to aggregation. Given the clear effect of the K19del mutation on CHP1 expression, we investigated the cellular localization of WT and mutant CHP1-GFP–tagged proteins in N2A (figure 3A), PC12, and HeLa cells (figure e-3, A and B, links.lww.com/NXG/A30) via fluorescence microscopy.

CHP1-WT-GFP staining displayed a uniform distribution throughout the cells, including neurite-like structures in N2A and PC12 cells (figure 3A and figure e-3A, links.lww.com/NXG/A30), whereas CHP1-K19del-GFP expression led to massive protein aggregates, which on detailed observation revealed 2 distinct patterns: small puncta-like structures and large amorphous accumulations with a very strong fluorescent signal. These aggregates were observed in cell body and neurite-like projections (figure 3A). Quantification of total accumulation/aggregation events in N2A cells showed that ~50% of CHP1-K19del-GFP cells presented aggregates compared with ~20% in CHP1-WT-GFP cells. Large aggregations were detected almost exclusively in CHP1-K19del-GFP cells (~22% vs ~4% in the WT; $p < 0.001$) (figure 3A). Similar accumulation patterns were observed in PC12 and HeLa cells (figure e-3, A and B, links.lww.com/NXG/A30).

To further characterize these abnormal protein aggregates, CHP1-WT– and K19del-GFP–expressing cells were stained for protein homeostasis markers such as ubiquitin and P62[27–29] (figure 3, B and C). Larger aggregates displayed positive colocalization and extensive accumulation of both markers, indicating that these structures are recognized by neuronal protein quality control systems, thus explaining CHP1-K19del–reduced expression. Altogether, these

Figure 2 **The K19del mutation affects the expression and solubility of CHP1**

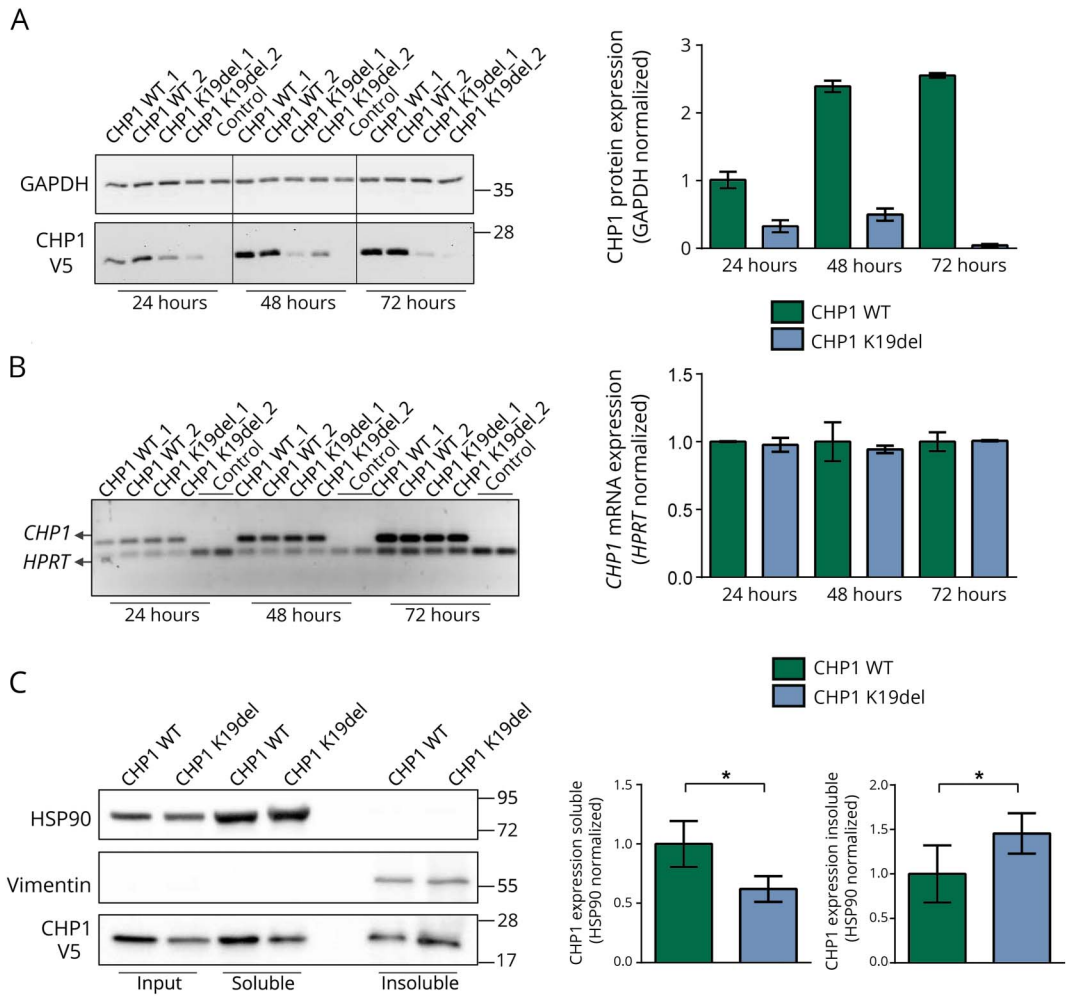

(A) Western blot (WB) from HEK293T lysates transiently expressing CHP1-WT-V5, CHP1-K19del-V5, or empty V5-vector (control) collected 24, 48, and 72 hours after transfection. Protein lysates were probed with antibodies against V5 to detect CHP1-WT and mutant proteins, and GAPDH as loading control. Expression of CHP1-K19del-V5 is almost undetectable after 72 hours. The graph represents quantification of CHP1 relative expression over different time points. Bars show the mean ± SEM. (B) Determination of *CHP1-WT-V5* and *K19del-V5* transcripts by semiquantitative RT-PCR. The graph represents quantification of *CHP1-V5* transcripts normalized to *HPRT* expression. Bars show the mean ± SEM. Negligible differences were observed between WT and *CHP1-K19del* transcripts. (C) Subcellular fractionation of protein lysates from HEK293T transiently overexpressing CHP1-WT-V5 or CHP1-K19del-V5 48 hours after transfection. Lysates were separated into soluble (cytoplasmic) and insoluble (cytoskeletal) fractions by differential lysis and centrifugation. Representative WB from total lysates and fractions were probed with V5 antibodies to detect CHP1-WT and mutant proteins. HSP90 and Vimentin were used as enrichment markers for soluble and insoluble fractions, respectively. Graphs represent quantification of relative expression of CHP1 in the soluble and insoluble fractions. Bars show the mean ± SEM from 3 independent blots. "*" denotes statistical significance ($p \leq 0.05$ two-tailed Student *t* test) between CHP1-WT and CHP1-K19del expression. GAPDH = glyceraldehyde 3-phosphate dehydrogenase; HPRT = hypoxanthine-guanine phosphoribosyltransferase; WT = wild type.

results strongly indicate that K19del causes an increased proneness of CHP1 to aggregation, potentially attributable to misfolding and/or structural protein defects.

The K19del mutation alters CHP1 association into functional complexes and impairs NHE1 membrane targeting. To conclusively confirm that the K19del mutation leads to formation of higher molecular size CHP1 species, we performed SEC. Elution profiles of CHP1-WT-V5 and K19del-V5 proteins were determined by V5-immunoblotting. CHP1-WT-V5 eluted in 2 regions, representing the monomeric CHP1 form (~25 KDa)[30,31] and the high-molecular-weight (HMW) complexes (~1 MDa). By contrast, the CHP1-K19del-V5 elution profile shifted not only away from the monomeric range toward higher fractions but also appeared in HMW fractions in which CHP1-WT is absent (figure 4A and e-4A). NHE1 elution also showed marked differences. A unique band was detected

Figure 3 **Protein aggregation in N2A cells expressing mutant CHP1**

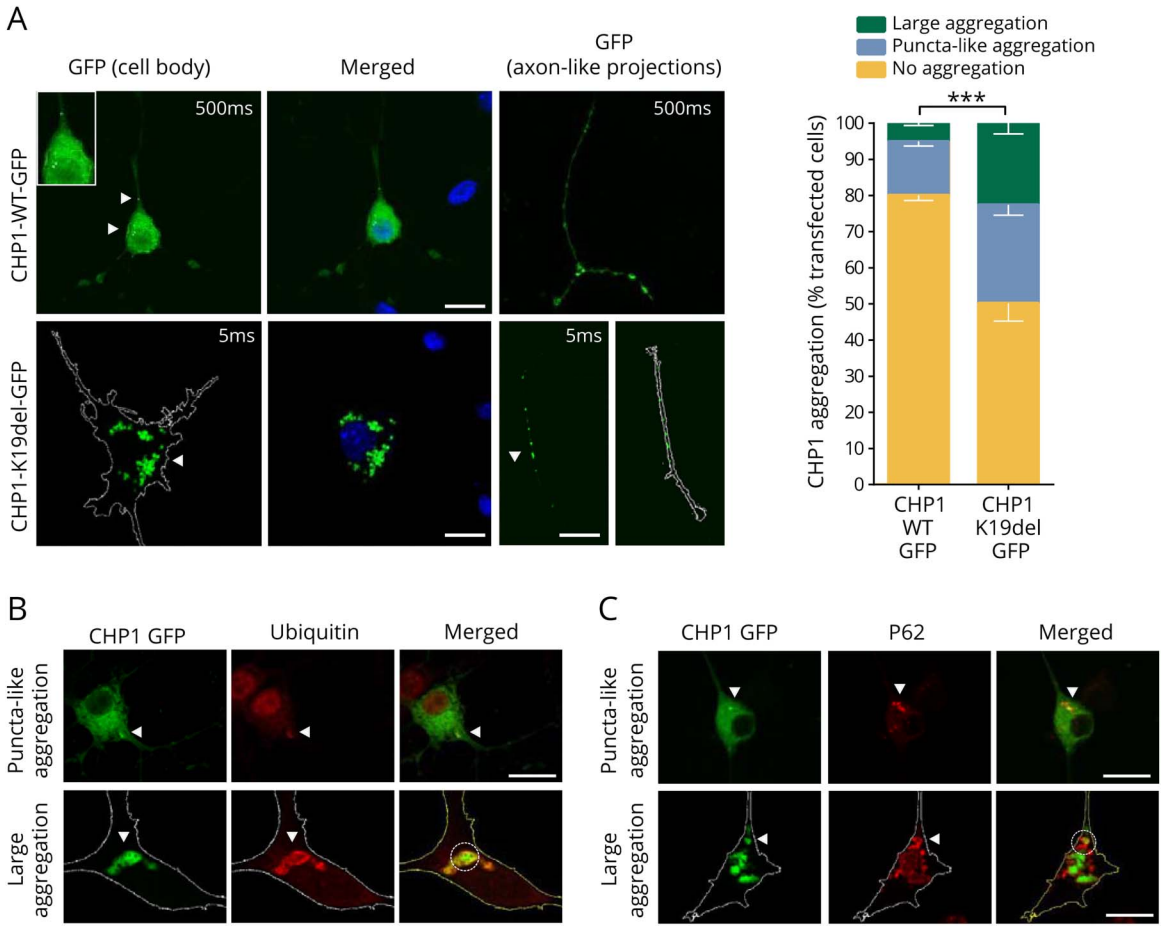

(A) Representative images of differentiated N2A cells transiently expressing CHP1-WT-GFP or CHP1-K19del-GFP proteins. CHP1-WT-GFP appears uniformly expressed both in the cell body and neurite-like structures of N2A cells. Small puncta-like aggregates are visible. CHP1-K19del-GFP expression leads to formation of large protein aggregations, both in the cell body and throughout axon-like projections. Puncta-like and large aggregations are indicated with white arrowheads. GFP exposure time in milliseconds is indicated inside the panels. Scale bar: 20 μm. The graph represents aggregation quantification in GFP-positive cells. Bars show the mean ± SEM from 6 independent experiments ($n \geq 250$). "***" denotes statistical significance ($p < 0.001$ χ^2 test). (B and C) CHP1-K19del aggregates colocalize with protein homeostasis markers. N2A cells expressing CHP1-WT-GFP or CHP1-K19del-GFP proteins were immunostained with ubiquitin and P62 antibodies. Representative images of puncta-like and large aggregations are depicted. Costes-adjusted Pearson colocalization coefficients were calculated for large aggregates, areas depicted in open circles: ubiquitin $p = 0.9$ and P62 $p = 0.85$. Positive coefficients indicate that aggregates colocalize with ubiquitin and P62. Scale bar: 20 μm. GFP = green fluorescent protein; WT = wild type.

in CHP1-WT HMW fractions, while 3 bands were observed for CHP1-K19del. Immunoblotting of glyceraldehyde 3-phosphate dehydrogenase, an interacting partner of CHP1,[32] did not show differences between CHP1-WT and mutant elution profiles (figure e-4A, links.lww.com/NXG/A30). These results demonstrate that additional higher molecular complexes of CHP1-K19del-V5 are formed, which result from the unspecific aggregation proneness of mutant CHP1.

Characterization studies of the CHP1-NHE1 complex demonstrate that this calcium-dependent interaction exclusively involves 8 specific residues of the aJ helix of the C-terminal region of CHP1.[7,30] These findings excluded the possibility of a direct implication of K19 in the interaction between both proteins. Examination of the crystal structure of CHP1[30] revealed that K19 is localized on the CHP1 first N-terminal Aα helix (figure 4B). Of interest, comparison of this structure with an NMR-generated CHP1-NHE1 segment complex structure[33] indicated that CHP1-Aα undergoes large conformational changes on NHE1 binding, forming a clamp fixating NHE1-C-terminal segment (figure 4B). Although the structure-function relationship of this feature is poorly understood, this structural analysis suggests that K19del could interfere with a fully functional CHP1-NHE1 complex formation impairing NHE1 targeting to the membrane or compromising the function of this complex.

Since membrane localization of CHP1 is dependent of NHE1,[6] but also membrane expression and maturation of NHE1 is reliant on CHP1,[34] we investigated the effect of CHP1-K19del on NHE1 membrane targeting. Thereby, membrane fractions from HEK293T cells

Figure 4 **K19del mutation alters CHP1 association into functional complexes, impairs NHE1 membrane targeting, and potentially compromises protein conformational changes**

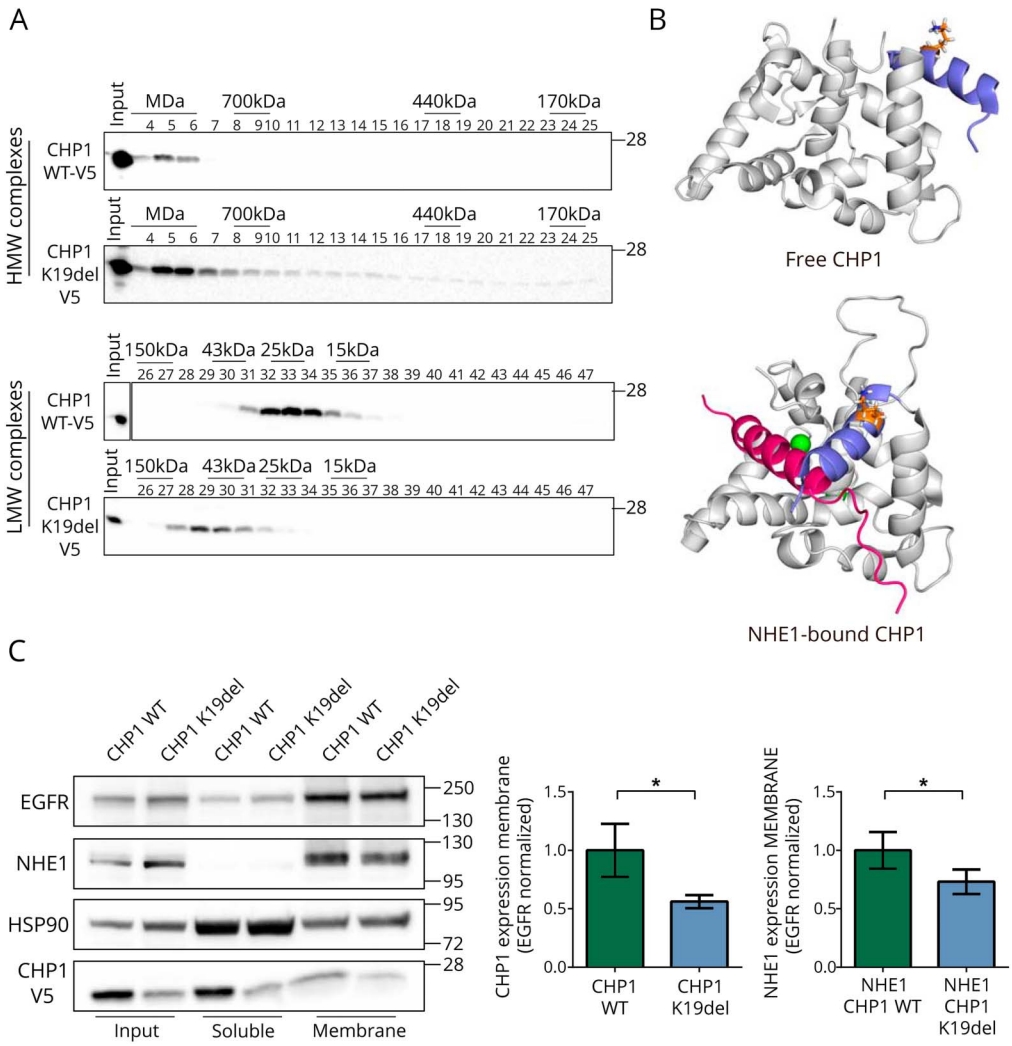

(A) Size-exclusion chromatography of total protein lysates from HEK293T cells expressing CHP1-WT-V5 and CHP1-K19del-V5. 42 protein fractions, 21 in the range of high molecular weight (HMW) and 21 in low molecular weight (LMW) were analyzed by Western blot (WB). Blots were probed with V5 antibodies to detect CHP1 WT and mutant proteins. Marked elution differences between WT and mutant CHP1 in both HMW and LMW complexes (fractions 7–25) are visible. CHP1-K19del-V5 elution in LMW fractions shifted to higher MW (29–30), away from the most abundant monomeric range (32–34). (B) Cartoon representation of the crystal structure of *Rattus norvegicus* free CHP1 (PDB code 2CT9) and *Homo sapiens* NMR complex structure NHE1-bound CHP1 (PDB code 2E30). CHP1 is depicted in gray, the NHE1 segment in magenta, and Ca^{2+} ions in green. The CHP1 Aα helix (residues 1 to 23) is depicted in blue and the K19 residue is shown in orange sticks. Note the open conformation of the CHP1 Aα helix in the free CHP1 structure and its closed-to-NHE1 hydrophobic pocket in the CHP1-bound structure. (C) Subcellular fractionation of protein lysates from HEK293T transiently overexpressing CHP1-WT-V5 and CHP1-K19del-V5 proteins. Fractions were separated into soluble (cytoplasmic) and membrane fractions by differential lysis and centrifugation. Representative WB of total lysates and fractions were probed with V5 antibodies to detect CHP1-WT and mutant proteins and NHE1. HSP90 and EGFR were used as enrichment markers for soluble and membrane fractions, respectively. Graphs represent quantification of relative expression of CHP1 and NHE1 in the membrane fraction. Bars show the mean ± SEM (error bars) from 3 independent blots. "*" denotes statistical significance ($p \leq 0.05$ Student *t* test). EGFR = Epidermal Growth Factor Receptor; WT = wild type.

expressing CHP1-WT– and K19del-V5–tagged proteins were analyzed by WB. In line with reduced cytoplasmic levels, CHP1-K19del membrane expression was also markedly diminished (figure 4C). It is important that marked NHE1 reduction in membrane fractions was observed on OE of mutant CHP1 (figure 4C), implying that CHP1-K19del interferes with proper NHE1 membrane targeting. Similar results were seen in N2A cells (figure e-4B, links.lww.com/NXG/A30).

***chp1* downregulation in zebrafish causes motor axon, cerebellar, and movement defects, which are rescued by wt, but not mutant CHP1 mRNA.** To analyze the pathogenic consequences of the hypomorphic CHP1-K19del

Figure 5 **Chp1 downregulation in zebrafish leads to CaP-MN, cerebellar, and movement defects rescued with WT, but not mutant *CHP1* mRNA**

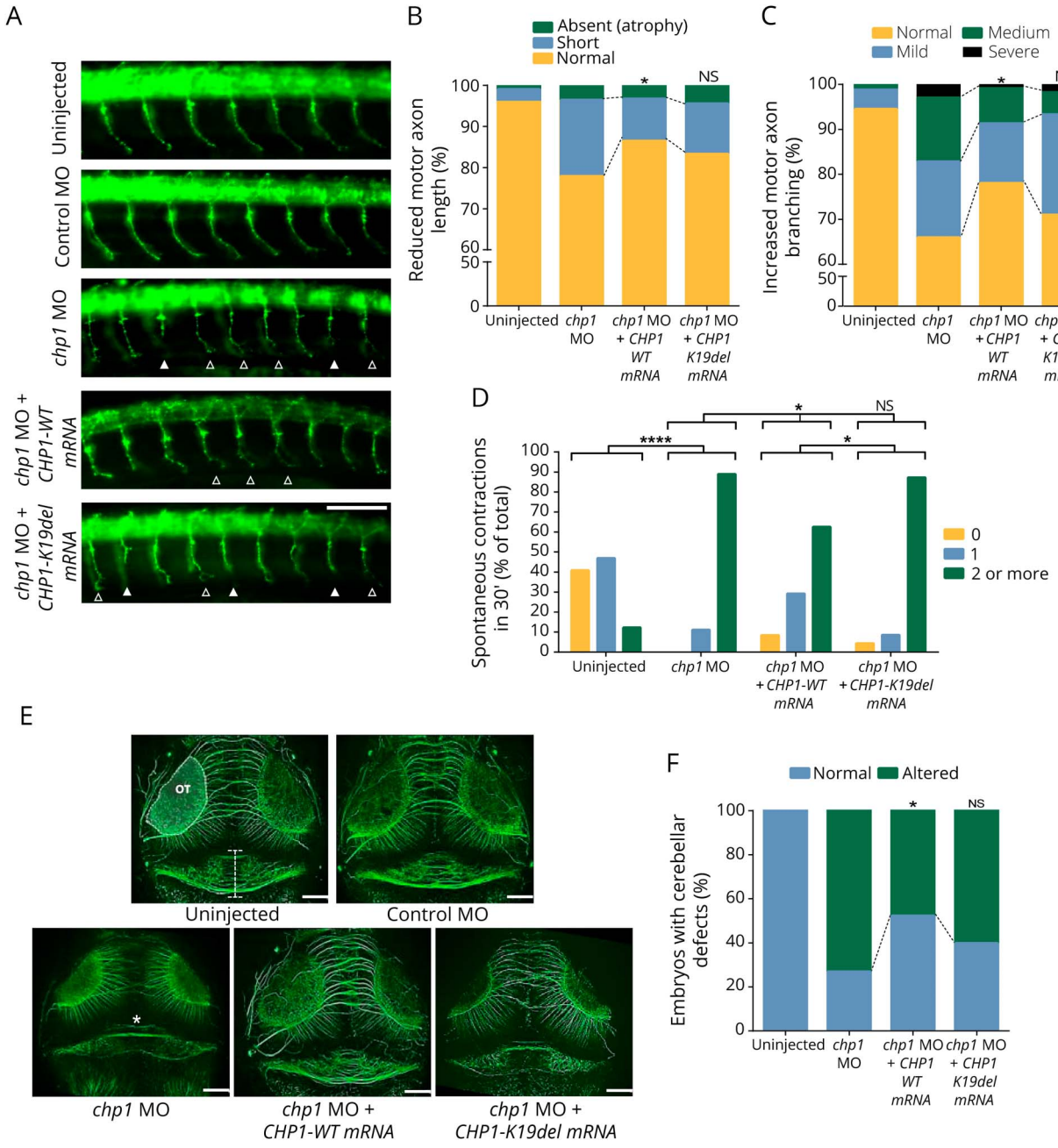

(A) Lateral views of whole-mount embryos stained with synaptotagmin antibody (znp1). Truncated and absent motor axons are indicated with solid arrowheads and terminally branched axons with open arrowheads. Scale bar: 25 μm. (B and C) Based on overall appearance, CaP-MNs were classified as follows: normal, short (truncated axonal projection), or absent (total axonal atrophy). Based on terminal branching, axons were classified as normal, mild (branching ventral from midline), medium (2–3 or more branches at ventral or midline), or severe (>3 branches ventral or dorsal from midline). *chp1*-depleted zebrafish larvae display CaP-MN truncations and increased terminal branching in comparison with control (non-targeting) Morpholino (MO) and uninjected fish. Quantitative analysis of CaP-MN demonstrates that coinjection of *chp1* MO and *CHP1-WT* mRNAs significantly improves axonal defects. Coinjection of *chp1* MO and *CHP1-K19del* mRNAs fails to ameliorate CaP-MN defects in comparison with *CHP1-WT* mRNA. Results are presented in percentages from $n \geq 150$ analyzed axons representing 3 independent experiments. * denotes statistical significance in comparison with the *chp1* MO group ($p \leq 0.05$ χ^2 test). (D) *chp1*-depleted ~34 hpf morphants show an increased frequency of spontaneous contractions. For graphic representation, spontaneous contractions were categorized as follows: 0 (no contraction), 1 (1 contraction in 30 seconds), and 2 or more (2 or more contractions in 30 seconds). Results are presented as the percentage of total from $n \geq 50$ observed zebrafish larvae representing 3 independent experiments. Coinjection of *chp1* MO and *CHP1-WT* mRNAs, but not *CHP1-K19-del* mRNA, significantly reduced spontaneous contractions in 30 seconds "****" denotes statistical significance ($p < 0.0001$ Fisher exact test). (E) Dorsal views of whole-mount embryos labeled with acetylated tubulin at ~72 hpf. The structure depicted between white horizontal lines in the uninjected morphant indicates the cerebellar area of observation. Optic tectum (OT) is outlined. Severe cerebellar hypoplasia is observed in *chp1*-depleted zebrafish in comparison with control MO and uninjected fish. "*" in *chp1* MO image indicates trochlear decussation. Scale bar: 25 μm. (F) Quantitative analysis of cerebellar defects demonstrates that coinjection of *chp1* MO and *CHP1-WT* mRNAs significantly ameliorates this phenotype. Coinjection of *chp1* MO and *CHP1-K19del* mRNAs fails to improve cerebellar defects to WT levels. Results are presented in percentages from $n \geq 40$ observed zebrafish morphants from 3 independent experiments. "*" denote statistical significance ($p \leq 0.05$ Fisher exact test). CaP-MN = caudal primary motor neuron; mRNA = messenger RNA; NS = not significant; WT = wild type.

mutation in vivo, we used MO to inhibit *chp1* translation in zebrafish. Different MO concentrations were injected to select a dosage with little effect on overall morphology and development, but quantifiable neurologic readout (figure e-5, A–D, links.lww.com/NXG/A30). MO efficacy was confirmed by WB (figure e-5E, links.lww.com/NXG/A30).

Chp1 deficiency resulted in CaP-MN defects, namely axonal truncations and increased terminal branching. In detail, ~23% of the analyzed CaP-MNs exhibited defects in axonal projection and ~35% showed increased terminal branching (figure 5, A–C). Furthermore, Chp1 reduction led to severe cerebellar hypoplasia in ~70% of the morphants. Trochlear decussation became visible on severe cerebellar reduction, and reduced size of the optic tectum was also observed but not included for quantification analyses (figure 5, E and F). Negligible CaP-MN impairments and no cerebellar defects were observed in control groups (figure e-5, B–D, links.lww.com/NXG/A30). Since individuals carrying *CHP1* mutation exhibit spastic paraparesis, gait instability, and ataxia (table e-3, links.lww.com/NXG/A29), we additionally examined *chp1* morphants movement in detail. Chp1 deficiency led to increased spontaneous contractions (figure 5D and video e-1, links.lww.com/NXG/A31) and to abnormal spastic-like trunk movement unaccompanied of locomotion (video e-2, links.lww.com/NXG/A32).

To corroborate *chp1*-MO phenotype specificity and confirm CHP1-K19del pathogenicity, rescue experiments were performed using WT and mutant *CHP1*-mRNAs. Protein OE was confirmed by WB (figure e-5F, links.lww.com/NXG/A30), and neither CaP-MN nor cerebellar defects were observed on *CHP1*-mRNAs OE (figure e-5, B–D, links.lww.com/NXG/A30). Coinjection of *chp1* MO and *CHP1-WT* mRNA, but not *CHP1-K19del* mRNA, ameliorated all neurologic and movement defects associated with Chp1 deficiency ($p \leq 0.05$). Thus, *CHP1-WT* mRNA improved axonal truncations, terminal branching, and cerebellar hypoplasia by ~13%–20% and 25%, respectively, compared with *chp1* MO alone (figure 5, A–C, E and F). Spontaneous contractions were partially restored to uninjected larvae levels (figure 5D). Rescue experiments did not fully reach control levels probably because of the limited expression of synthetic mRNAs.[35] Together, the neurologic and movement defects observed in *chp1* morphants validate CHP1 reduction as the underlying cause of MN defects and ratify cerebellar hypoplasia as the central pathogenic feature underpinning CHP1 pathogenesis.

DISCUSSION Following a combination of exome and linkage analysis in a consanguineous family, we identified a 3-bp deletion in a highly conserved domain of *CHP1* as a novel cause of ARCA. Neither focused *CHP1* screening in 2 large cohorts with ARCA and NMD nor interrogating GeneMatcher[20] unraveled a second mutation, emphasizing the scarcity of *CHP1* variants. This is further underpinned by the reduced tolerability for missense mutation found in control population (Exome Aggregation Consortium *z*-score: 2.64) and the high degree of conservation among CHP1 orthologs (99% amino acid identity in mouse and 92% in zebrafish).

Here, we demonstrated that CHP1-K19del severely affects protein expression and localization, thereby impairing NHE1 membrane expression, and consequently its function.[36] Therefore, CHP1 mutation causes ataxia, most likely, in an NHE1-dependent manner (figure e-6, A and B, links.lww.com/NXG/A30), resembling the mechanism of cerebellar degeneration described for *Chp1 vacillator*[6] and *Nhe1* KO mice.[9] Albeit aggregation is inherent to misfolded proteins in neurodegenerative disease,[29] the aggregation proneness described for CHP1-K19del should be considered as a readout of abnormal protein folding rather than a disease mechanism itself.

The affected siblings of this study present with cerebellar atrophy and motor neuropathy, which were recapitulated in zebrafish. c*hp1* morphants exhibited severe cerebellar hypoplasia and CaP-MN alterations, thus demonstrating that MNs are also compromised on CHP1 downregulation. Moreover, Chp1 reduction in zebrafish resulted in increased spontaneous contractions and spastic-like trunk movements, supporting that CHP1 deficiency underlies the spastic phenotype in humans. Although the common denominator between *Chp1* and *Nhe1* mouse models is Purkinje cell degeneration, other central nervous areas such as the hippocampus and hypothalamus are also sensitive to NHE1 depletion.[37,38] We speculate that abundant NHE1 expression in MN[39] and MN precursors[40] might regulate the proclivity of this population to CHP1 misbalance. In contrast to the CHP1-deficient associated phenotype, NHE1 deficiency was presumptively associated with hearing loss, despite that neither *Nhe1* nor *Chp1* models presented deafness. More strikingly, depletion of mouse *Nhe1* results in ataxia and epilepsy, while patients with LKS do not present with episodic seizures.[6,9] This phenotypic variability strongly suggests that differential NHE1 dosages finely tune different pathogenic outcomes. Notably, CHP1-K19del reduces but not abolishes CHP1 expression, thereby NHE1 membrane targeting is reduced, but not fully compromised. We hypothesize, in conformity with others,[11] that reduced NHE1 certainly leads to ataxia, but remaining levels are sufficient to protect patients with *CHP1* mutations from epilepsy or deafness as in patients

with LKS. Moreover, tissue-specific expression of other CHP or NHE proteins could modulate phenotypic compensations, further explaining the incomplete phenotypic translation from mouse to humans and the variability among human phenotypes.

AUTHOR CONTRIBUTIONS

Designing the study, drafting the manuscript, data interpretation, and study supervision: N.M.-F. and B.W. Functional experiments, data acquisition, processing, and analysis: N.M.-F. with help from E.J., S. H., H.L., S.S., J.M., M.R., C.P., L.T.-B., and M.H. Clinical evaluation and follow-up of patients: A.D. and A.B. Genetic and linkage analysis and data interpretation: M.C., M.K., G.S., A.S., and S.Z. Revising and approving the manuscript: all authors.

ACKNOWLEDGMENT

The authors thank all participating family members, the IGenSeq facility, and the DNA and Cell Bank of the Institut du Cerveau et de la Moelle épinière. They also thank Markus Storbeck for support in protocols and experimental details; Isabelle Le Ber and Andrea Delle Vedove for advice in medical details; and Monia B Hammer for genotype analysis. M.C. was the recipient of a fellowship from the Fond National de la Recherche Scientifique (aspirant FNRS).

STUDY FUNDING

FP7/2007-2013 under agreement 2012-305121 (NEUROMICS, to B.W. and A.B.), Center for Molecular Medicine Cologne (CMMC C11 and C16 to B.W.), Deutsche Forschungsgemeinschaft (Wi945/14-2, Wi945/16-1 to B.W.), the French National Agency for Research (SPATAX-QUEST, ANR-13-ISV1-0002 to G.S.), the ERARE-3 Joint Transnational Call grant "Preparing therapies for autosomal recessive ataxias" (PREPARE, ANR-16-RAR3-0011-03 to G.S. and S.Z.), the French Ministry of Health (PHRC 2009, AOM 09178 to A.D.), the VERUM Foundation (to A.B. and G.S.), the Fondation Roger de Spoelberch (to A.B.), the Association Connaitre les Syndromes Cérébelleux (to G.S.), and benefited from the Programme Investissements d'Avenir ANR-10-IAIHU-06 (to the ICM Institute).

DISCLOSURE

N. Mendoza-Ferreira co-holds patent 17172826.4-1401 (European patent office) for Calcineurin B homologous protein 1 inhibitors and therapeutic and non-therapeutic uses thereof. M. Coutelier has received research support from Fonds National de la Recherche Scientifique (F.R.S.-FNRS). E. Janzen and S. Hosseinibarkooie co-hold patent 17172826.4-1401 (European patent office) for Calcineurin B homologous protein 1 inhibitors and therapeutic and non-therapeutic uses thereof. H. Löhr, S. Schneider, J. Milbradt, and M. Karakaya report no disclosures. M. Riessland patented the use of specific antisense oligonucleotides to block NCALD expression to treat SMA. C. Pichlo and L. Torres-Benito report no disclosures. A. Singleton has received travel funding from 23andMe; serves on the editorial boards of *Annals of Neurology*, *Lancet Neurology*, *Neurogenetics*, *Neurodegenerative Diseases*, *Brain*, and the *Journal of Parkinson's Disease* (no financial compensation); has a patent pending for panel of markers to diagnose stroke; and has received research support from NIH Intramural funding and Department of Defense. S. Zuchner reports no disclosures. A. Brice has served on the scientific advisory boards of FWO (Research Foundation—Flanders), ERC (European Research Council), and BMBF (Bundesministeriums für Bildung und Forschung—Berlin, Germany); has served on the editorial boards of *Neurology and Clinical Neuroscience*, *Parkinsonism & Related Disorders*, *Brain*, *Neurodegenerative Diseases*, *The Cerebellum*, and *Neurogenetics*; and has received research support from French Research Agency (EU), the French program, FP (France Parkinson Association), RDS (Roger de Spoelberch Foundation), FDF (Fondation de France), and FRM (Fondation pour la Recherche Médicale). A. Durr has served on the scientific advisory boards of INSERM (National Institute for Health and Research), the Helmholtz Initiative on Personalized Medicine—Germany, the Grenoble Neuroscience Institute of Grenoble, and the France Board of Directory of the ENP; has served on the editorial boards of *Neurology® Genetics* and *Journal of Huntington's Disease*; has served on the International Advisory Committee of *Archives of Neurology*; co-holds a patent and receives royalty payments for Anaplerotic therapy of Huntington disease and other polyglutamine diseases (BIO06353 Mochel/Durr [EP 06291873.5, April 12, 2006]); has been a consultant for Roche and Brainvectis; and has received research support from CoEn 2015: WIN-HD—Decoding Presymptomatic white matter changes in Huntington Disease 2015–2018. M. Hammerschmidt has served on the editorial boards of *Development, Genes and Evolution* and *Molecular Genetics and Genomics*; and has received research support from the National Institute of General Medicine Sciences and Deutsche Forschungsgemeinschaft. G. Stevanin has received travel funding from the Movement Disorder Society; holds patents for Diagnosis of hereditary spastic paraplegias (HSP) by identification of a mutation in the KIAA1840 gene or protein and for Diagnosis of hereditary spastic paraplegias (HSP) by identification of a mutation in the ZFYVE26 gene or protein; and has received research support from the European Community's Seventh Framework Program, French Agency for Research, Erare Programme 2013–2018, Erare Programme 2016–2019, the program "Investissements d'Avenir," Association Strümpell-Lorrain France, and Association Connaitre les Syndromes Cérébelleux. B. Wirth has served on the scientific advisory board of SMA Europe; has received travel funding and speaker honoraria from Biogen; co-holds patent 17172826.4-1401 (European patent office) for Calcineurin B homologous protein 1 inhibitors and therapeutic and non-therapeutic uses thereof; and has received research support from the European Community's Seventh Framework Program. Go to Neurology.org/ng for full disclosure forms.

Received August 11, 2017. Accepted in final form August 22, 2017.

REFERENCES

1. Filla A, De Michele G. Overview of autosomal recessive ataxias. Handb Clin Neurol 2012;103:265–274.
2. Anheim M, Fleury M, Monga B, et al. Epidemiological, clinical, paraclinical and molecular study of a cohort of 102 patients affected with autosomal recessive progressive cerebellar ataxia from Alsace, Eastern France: implications for clinical management. Neurogenetics 2010;11:1–12.
3. Sailer A, Houlden H. Recent advances in the genetics of cerebellar ataxias. Curr Neurol Neurosci Rep 2012;12: 227–236.
4. Coutelier M, Stevanin G, Brice A. Genetic landscape remodelling in spinocerebellar ataxias: the influence of next-generation sequencing. J Neurol 2015;262:2382–2395.
5. Sawyer SL, Schwartzentruber J, Beaulieu CL, et al. Exome sequencing as a diagnostic tool for pediatric-onset ataxia. Hum Mutat 2014;35:45–49.
6. Liu Y, Zaun HC, Orlowski J, Ackerman SL. CHP1-mediated NHE1 biosynthetic maturation is required for Purkinje cell axon homeostasis. J Neurosci 2013;33: 12656–12669.
7. Pang T, Hisamitsu T, Mori H, Shigekawa M, Wakabayashi S. Role of calcineurin B homologous protein in pH regulation by the Na+/H+ exchanger 1: tightly bound Ca2+ ions as important structural elements. Biochemistry 2004;43:3628–3636.
8. Putney LK, Denker SP, Barber DL. The changing face of the Na+/H+ exchanger, NHE1: structure, regulation, and cellular actions. Annu Rev Pharmacol Toxicol 2002; 42:527–552.
9. Cox GA, Lutz CM, Yang CL, et al. Sodium/hydrogen exchanger gene defect in slow-wave epilepsy mutant mice. Cell 1997;91:139–148.
10. Bell SM, Schreiner CM, Schultheis PJ, et al. Targeted disruption of the murine Nhe1 locus induces ataxia,

growth retardation, and seizures. Am J Physiol 1999;276: C788–C795.
11. Guissart C, Li X, Leheup B, et al. Mutation of SLC9A1, encoding the major Na(+)/H(+) exchanger, causes ataxia-deafness Lichtenstein-Knorr syndrome. Hum Mol Genet 2015;24:463–470.
12. Margolin DH, Kousi M, Chan YM, et al. Ataxia, dementia, and hypogonadotropism caused by disordered ubiquitination. N Engl J Med 2013;368:1992–2003.
13. Akizu N, Cantagrel V, Zaki MS, et al. Biallelic mutations in SNX14 cause a syndromic form of cerebellar atrophy and lysosome-autophagosome dysfunction. Nat Genet 2015;47:528–534.
14. Kawahara G, Hayashi YK. Characterization of zebrafish models of Marinesco-Sjogren syndrome. PLoS One 2016;11:e0165563.
15. Abecasis GR, Cherny SS, Cookson WO, Cardon LR. Merlin—rapid analysis of dense genetic maps using sparse gene flow trees. Nat Genet 2002;30:97–101.
16. Riessland M, Kaczmarek A, Schneider S, et al. Neurocalcin delta suppression protects against spinal muscular atrophy in humans and across species by restoring impaired endocytosis. Am J Hum Genet 2017;100:297–315.
17. Flanagan-Steet H, Fox MA, Meyer D, Sanes JR. Neuromuscular synapses can form in vivo by incorporation of initially aneural postsynaptic specializations. Development 2005;132:4471–4481.
18. Hoyt C. Rapid, high-throughput homogenization of embryonic or larval zebrafish (*Danio rerio*). Protocol Exchage 2009. Available at http://dx.doi.org/10.1038/nprot.2009.211.
19. Lim J, Hao T, Shaw C, et al. A protein-protein interaction network for human inherited ataxias and disorders of Purkinje cell degeneration. Cell 2006;125:801–814.
20. Sobreira N, Schiettecatte F, Valle D, Hamosh A. GeneMatcher: a matching tool for connecting investigators with an interest in the same gene. Hum Mutat 2015;36:928–930.
21. Holmes G. A form of familial degeneration of the cerebellum. Brain 1908;30:466–489.
22. Abs R, Van Vleymen E, Parizel PM, Van Acker K, Martin M, Martin JJ. Congenital cerebellar hypoplasia and hypogonadotropic hypogonadism. J Neurol Sci 1990;98:259–265.
23. Pierce SB, Walsh T, Chisholm KM, et al. Mutations in the DBP-deficiency protein HSD17B4 cause ovarian dysgenesis, hearing loss, and ataxia of Perrault syndrome. Am J Hum Genet 2010;87:282–288.
24. Ma J, Zeng F, Schultz RM, Tseng H. Basonuclin: a novel mammalian maternal-effect gene. Development 2006;133: 2053–2062.
25. Zhang X, Chou W, Haig-Ladewig L, et al. BNC1 is required for maintaining mouse spermatogenesis. Genesis 2012;50:517–524.
26. Tsuiko O, Noukas M, Zilina O, et al. Copy number variation analysis detects novel candidate genes involved in follicular growth and oocyte maturation in a cohort of premature ovarian failure cases. Hum Reprod 2016;31: 1913–1925.
27. Kopito RR. Aggresomes, inclusion bodies and protein aggregation. Trends Cell Biol 2000;10:524–530.
28. Zatloukal K, Stumptner C, Fuchsbichler A, et al. p62 Is a common component of cytoplasmic inclusions in protein aggregation diseases. Am J Pathol 2002;160:255–263.
29. Taylor JP, Hardy J, Fischbeck KH. Toxic proteins in neurodegenerative disease. Science 2002;296:1991–1995.
30. Naoe Y, Arita K, Hashimoto H, Kanazawa H, Sato M, Shimizu T. Structural characterization of calcineurin B homologous protein 1. J Biol Chem 2005;280:32372–32378.
31. Timm S, Titus B, Bernd K, Barroso M. The EF-hand Ca (2+)-binding protein p22 associates with microtubules in an N-myristoylation-dependent manner. Mol Biol Cell 1999;10:3473–3488.
32. Andrade J, Pearce ST, Zhao H, Barroso M. Interactions among p22, glyceraldehyde-3-phosphate dehydrogenase and microtubules. Biochem J 2004;384:327–336.
33. Mishima M, Wakabayashi S, Kojima C. Solution structure of the cytoplasmic region of Na+/H+ exchanger 1 complexed with essential cofactor calcineurin B homologous protein 1. J Biol Chem 2007;282:2741–2751.
34. Matsushita M, Tanaka H, Mitsui K, Kanazawa H. Dual functional significance of calcineurin homologous protein 1 binding to Na(+)/H(+) exchanger isoform 1. Am J Physiol Cell Physiol 2011;301:C280–C288.
35. Pyati UJ, Look AT, Hammerschmidt M. Zebrafish as a powerful vertebrate model system for in vivo studies of cell death. Semin Cancer Biol 2007;17:154–165.
36. Matsushita M, Sano Y, Yokoyama S, et al. Loss of calcineurin homologous protein-1 in chicken B lymphoma DT40 cells destabilizes Na+/H+ exchanger isoform-1 protein. Am J Physiol Cell Physiol 2007;293:C246–C254.
37. Ma E, Haddad GG. Expression and localization of Na+/H+ exchangers in rat central nervous system. Neuroscience 1997;79:591–603.
38. Gu XQ, Yao H, Haddad GG. Increased neuronal excitability and seizures in the Na(+)/H(+) exchanger null mutant mouse. Am J Physiol Cell Physiol 2001;281: C496–C503.
39. Yang Y, Xie Y, Chai H, et al. Microarray analysis of gene expression patterns in adult spinal motoneurons after different types of axonal injuries. Brain Res 2006;1075:1–12.
40. Satoh J, Asahina N, Kitano S, Kino Y. A comprehensive profile of ChIP-seq-based Olig2 target genes in motor neuron progenitor cells suggests the possible involvement of Olig2 in the pathogenesis of amyotrophic lateral sclerosis. J Cent Nerv Syst Dis 2015;7:1–14.